Influence of dissolved air on bubble attachment to highly oriented pyrolytic graphite

Marta Krasowska [1,2], Pasindu M. F. Sellapperumage [1,2], John Ralston [3], David A. Beattie [1,2]

[1] Future Industries Institute, University of South Australia, Mawson Lakes Campus, Mawson Lakes, SA 5095, Australia

[2] School of Information Technology and Mathematical Sciences, University of South Australia, Mawson Lakes Campus, Mawson Lakes, SA 5095, Australia

[3] Division of Information Technology, Engineering and the Environment, University of South Australia, Mawson Lakes, SA 5095, Australia

Corresponding author: marta.krasowska@unisa.edu.au (Marta Krasowska)

Abstract: The effect of air, dissolved in 0.1 M KCl solution, on bubble attachment to the smooth hydrophobic surface of highly oriented pyrolytic graphite was studied. The stability of a wetting film in such a system is governed by surface forces, i.e. electrostatic and van der Waals interactions. At the high ionic strength investigated, the electric double layer forces are both weak and of short range, therefore the stability of the wetting film is dominated by van der Waals interactions. The Hamaker coefficient for the highly oriented pyrolytic graphite-KCl aqueous solution-air system is negative and hence van der Waals interactions are repulsive. A repulsive force should stabilize the wetting film, preventing its rupture and bubble attachment to the highly oriented pyrolytic graphite surface. Many experimental studies have found that wetting films are not stable at graphite or coal surfaces, and air bubbles attach. In the present experiments, the stability of the wetting films decreased with increasing amount of dissolved air. The time required for film drainage, rupture, and air bubble attachment was shortened by two orders of magnitude when the experiments were performed in air saturated 0.1 M KCl solution. This instability was attributed to an increasing number of nano- and submicron- bubbles nucleated at the graphite surface. The Hamaker coefficient across the air-KCl aqueous solution-air system is positive and hence van der Waals interactions are attractive, resulting in wetting film rupture and macroscopic air bubble attachment to a highly oriented pyrolytic graphite surface decorated with resident nano- and submicro-metre bubbles.

Keywords: bubble attachment, hydrophobic surface, van der Waals interactions, nanobubbles, dissolved air

1. Introduction

The attachment of an air bubble to a solid surface is only possible if the thin liquid film (i.e. wetting film) between them ruptures, forming a perimeter large enough to prevent any subsequent detachment (Nguyen et al., 1998; Nguyen and Schulze, 2003; Krasowska and Malysa, 2007b). The stability of a wetting film, and hence the probability of bubble attachment, in a system where the probability of collision is 1 is governed by the interaction forces acting across such a film. The electrostatic component of the total force depends on the surface potential at the solid-solution and solution-air interfaces (Krasowska et al., 2007; Jiang et al. 2010) and, unless the experiments are carried out below the isoelectric point for the solid and above that for the bubble, the electric double layer forces will be repulsive and will act to stabilise the wetting film. In addition, the van der Waals interactions between an air bubble and a pristine solid surface in aqueous solution are short range and repulsive since the Hamaker coefficient is negative. The only exception is for solids of refractive index lower than refractive index of aqueous phase (Israelachvili, 2011), which is a very rare occurrence; in such a system the Hamaker coefficient is positive and hence the van der Waals interaction is attractive.

However, it is well known that the thin liquid film between an air bubble and a hydrophobic solid is generally unstable and ruptures, allowing bubble attachment to such a surface. To explain this phenomenon the concept of 'long range hydrophobic forces' was introduced (Israelachvili and Pashley, 1982; Israelachvili and Pashley, 1984; Yoon and Mao, 1996). Different mechanisms for these hydrophobic forces have been discussed and modeled, in particular: i) hydrogen-bond-propagated ordering of interfacial water molecules (Eriksson et al., 1989); and ii) bridging air nanobubbles between the hydrophobic surfaces (Parker et al., 1994; Stöckelhuber et al., 2004; Mishchuk et al., 2006). The latter mechanism is now generally accepted as the key to the origin of long range hydrophobic forces. Nano- and/or submicro-metre bubbles and/or continuous thin air films have been detected at hydrophobic solid surfaces immersed in aqueous solution using tapping mode Atomic Force Microscopy (Ishida et al., 2000; Lou et al., 2000; Lou et al., 2002; Simonsen et al., 2004; Zhang et al., 2006; Hampton and Nguyen, 2010; Craig, 2011), high-energy x-ray reflectivity experiments (Mezger et al., 2006), neutron reflectivity experiments (Steitz et al., 2003), nonintrusive optical interference-enhanced reflection microscopy (Karpitschka et al., 2012), optical microscopy using the total internal reflection fluorescence excitation (Chan and Ohl, 2012), and synchrotron-based scanning transmission soft X-ray microscopy (Zhang et al., 2013). Kinetics of the adsorption of CO_2 molecules (mimicking nucleation of air nano- and submicro-metre bubbles) dissolved in aqueous solution onto a hydrophobised silica surface were also investigated using attenuated total reflection Fourier transform infrared spectroscopy (Gong et al., 1999; German et al., 2014), and a quartz crystal microbalance (Yang et al., 2007).

Where a hydrophobic surface immersed in aqueous solution is partially covered with nano- or submicro-metre air bubbles, particularly where the electrical double layer is compressed due to high electrolyte concentration and the Debye length is much smaller than the typical height of nano-/submicro-metre bubbles, the initial wetting film (air bubble-aqueous solution-solid) resembles a foam film (air bubble-aqueous solution-air nano-/submicro-metre bubble). The Hamaker coefficient for a symmetric system is positive and the van der Waals interaction becomes attractive, rather than repulsive.

The amount and size of nucleated nanobubbles should depend on the amount of gas dissolved in the aqueous phase. Considine et al. measure the forces acting between two polystyrene latex spheres in aqueous media. They found out that the attractive force they measured was dependent on the amount of dissolved gas and its range decreased significantly when the level of dissolved gas in the water was reduced (Considine et al., 1999). Studies of aggregation rates and stability ratios allow the indirect assessment of interparticle forces (Trefalt et al., 2013). Snoswell et al. (Snoswell et al., 2003) studied the aggregation kinetics of hydrophilic and hydrophobic (methylated) silica particles in the presence of dissolved CO_2. They showed that hydrophobic particles underwent faster aggregation rates with increasing concentrations of dissolved carbon dioxide and concluded that "*Surface heterogeneity, both chemical and physical, and hydrophobicity promote the formation of gas bubbles. These very small surface bubbles are predicted to change both the van der Waals and electrostatic forces acting between the particles*".

Here we aim to investigate the effect of the dissolved air on the thin liquid film stability and the bubble attachment to atomically smooth, model hydrophobic surface of highly oriented pyrolytic graphite in 10^{-1} M KCl. The use of such a system allows us to rule out any effects arising from electric double layer forces, as well as solid surface roughness.

2. Materials and methods

Highly oriented pyrolytic graphite, HOPG, of SPI-1 grade (mosaic spread angle of 0.4° ± 0.1°) was purchased from SPI Supplies (USA) and used for all experiments. 1×1 cm² square surfaces were used for bubble-surface collision experiments, while discs of diameter of 1 cm were used to measure streaming potential. A fresh surface of HOPG was exposed by peeling the top layer of the mineral sample using clean tweezers and/or a scalpel blade prior to each experiment. HOPG was chosen as it is atomically smooth and any effects related to surface roughness are not present on such a surface. In reality there are some defects in the material, and the mosaicity, defects and granular structure

between HOPG samples may vary. This is dependent on how HOPG is made by the supplier (mostly the annealing temperature and times).

KCl (99%, AR) was purchased from Chem-Supply, Australia. KCl was calcined (550 °C for 8 hours), recrystallised, and calcined again (550 °C for 8 hours) to ensure removal of any surface active impurities. Three types of 10^{-1} M KCl solution with different air content were prepared using purified KCl and Milli-Q water (supplied by an Advantage A10 system from Millipore, USA, with a resistivity of 18.2 MΩ·cm, an interfacial tension of 72.4 mN/m at 22 °C, and a total organic carbon component of less than 4 mg/dm³). To prepare degassed 10^{-1} M KCl solution, Milli-Q water was boiled for 30 min and purified KCl was dissolved once the water cooled to room temperature. The ultrasonic removal of dissolved gas (for 30 min) was the last step. The normal 10^{-1} M KCl solution was prepared by dissolving purified KCl in Milli-Q water without any further treatment. The air saturated 10^{-1} M KCl solution was prepared by cooling Milli-Q water down to 4°C and then bubbling purified compressed air through a glass porous frit into the solution for 45 min. The pH of air saturated solution was 5.6. Therefore, to keep both ionic strength and pH constant, the pH values of degassed and normal 10^{-1} M KCl solutions were adjusted to 5.6 with 10^{-1} M and 10^{-2} M HCl (volumetric grade, Scharlau, Spain).

Bubble-surface collisions and the dewetting kinetics experiments on bare HOPG surfaces in degassed, normal and air saturated 10^{-1} M KCl solutions were carried out using a rising microbubble apparatus (Kor et al. 2014; Wu et al., 2015). Air bubbles (bubble radius, R_b, of 190 – 212 μm) were released by a microfluidic chip and allowed to rise in a borosilicate column of a square (30 mm×30 mm) cross-section filled with the 10^{-1} M KCl solutions containing different quantities of dissolved air. Air bubble collisions with either solution-air or solution-HOPG interfaces were recorded at ~ 8 cm above the point of bubble formation (i.e. at the point where the air bubble was moving with its terminal velocity) with a frequency of 2000 Hz using a high speed CCD camera (SA3, Photron) connected to a stereomicroscope (SZ-CTV, Olympus). Thirty collisions were recorded and analysed for each solution condition.

The Zeta potential, ζ, of HOPG was determined from streaming potential measurements using a rotating disc principle (Rogers and Lance, 1960). A ZetaSpin 2.0 instrument (Zetametrix, USA) was used. The HOPG surface was attached to a sample holder and placed in the measuring chamber 0.3 mm above the reference electrode. In order to minimize bubble presence/adhesion at the HOPG surface upon sample rotation, degassed solutions of 10^{-4} M, $5×10^{-4}$ M, 10^{-3} M, $5×10^{-3}$ M, and 10^{-2} M KCl at pH 5.6 were used during the experiments. The measured streaming potential is the jump in the voltage recorded as the motor switches the sample rotations (3000 RPM) from off to on and back off again. In order to avoid unsteady drift during sample rotation, the sample rotation rate was modulated by a square wave. The streaming potential was the average taken from 10 measurements. The zeta potential was determined using the following formula (Sides et al. 2006; Sides and Prieve 2013):

$$\zeta \cong \frac{1.96\kappa_l\eta^{1/2}}{\varepsilon_l d\Omega^{3/2}} \frac{1}{2\left(1-\frac{z}{d}-\frac{1}{2\left(\frac{z^2}{d^2}+1\right)^{1/2}}\right)} \phi_s \tag{1}$$

where: κ_l is the liquid conductivity, η is the kinematic liquid viscosity, ε_l is the liquid permittivity, d is the HOPG sample diameter, Ω is the sample rotation rate (in radians per second), z is the distance between the HOPG sample and the reference electrode and ϕ_s is the measured streaming potential.

All the measurements were carried out at T = 22±1 °C.

3. Results and discussion

To avoid kinetic effects such as the bubble bouncing off the solution-HOPG interface, the bubble collision experiments were carried out using air bubbles in the size range 190 μm < R_b < 212 μm, with R_b being the bubble radius. The Reynolds numbers, Re, for such bubbles are between 17 and 23. The terminal velocities of air bubbles rising in 10^{-1} M KCl solutions were measured from the difference in the air bubble position as a function of time. The terminal velocities for air bubbles in this size range were 38 – 49 mm/s. These experimentally measured terminal velocity values are in a good agreement

with the ones predicted by Klaseboer et al. for bubbles of $0 < Re < 500$ (Klaseboer et al. 2011) indicating that the air bubble surface is fully mobile and there are no adsorbing surface active impurities in our system (Malysa et al., 2005; Zawala et al., 2007; Malysa et al., 2011; Zawala et al., 2015).

Since solution degassing poses serious challenges in any experiments involving air bubbles, i.e. generated air bubbles can dissolve in the solution in order to restore the equilibrium, only 'mild' solution degassing (i.e. Milli-Q water boiling and ultrasonication) was used for bubble rise and collision experiments. The size of the first 15 air bubbles generated in degassed, normal and air saturated 10^{-1} M KCl solutions was measured as a function of the distance from the microfluidic chip outlet. There was no detectable bubble size decrease (for degassed 10^{-1} M KCl solution) nor increase (for air saturated 10^{-1} M KCl solution). The bubbles radii were, within the experimental error, the same for all three solutions.

The air bubbles rise at their terminal velocity before they approach the solution-air or solution-HOPG interface. When the air bubble approaches the interface its velocity starts to decrease approximately 1 bubble diameter away from the interface. A typical velocity profile as a function of bubble distance from the solution-air interface (normalized to bubble radius) is presented in Figure 1. For an air bubble of R_b = 198 μm, its terminal velocity (ca. 44 mm/s) decreases to ca. 38 mm/s when the bubble is one radius away from the free interface. The further decrease in velocity as the bubble approached the solution-air interface is even more apparent.
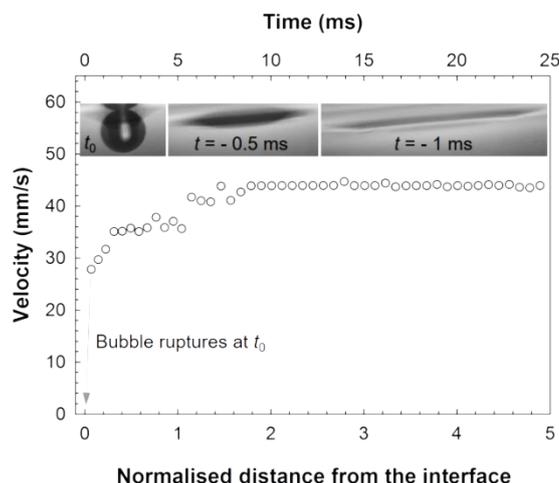
Fig. 1. Velocity of an air bubble (R_b = 198 μm) approaching the 0.1 M KCl-air interface as a function of its distance from the interface. The distance is normalized to R_b. The photos inserted in the top panel of the graph show the rapid (fraction of a millisecond) process of bubble coalescence, i.e. $t_0 = t_{rupture}$

When the air bubble touches the interface at t_0 (see the inserted sequence of photos in the top panel of Fig. 1) it bursts immediately, coalescing with the solution-air interface. The process is much quicker (i.e. fraction of a millisecond) than for larger air bubbles, i.e. for air bubbles of R_b = 740 μm the bubble coalescence time with the water-air interface, estimated from the moment when the bubble stays motionless, is ca. 3 ms (Zawala et al., 2015). Similar behaviour, i.e. a decrease in bubble velocity, is observed when the bubble approaches the solution-solid interface. Figure 2 shows a sequence of photos for a bubble colliding with a solution-HOPG interface in degassed (top panel of Figure 2), normal (middle panel of Fig. 2), and air saturated (top panel of Fig. 2) 10^{-1} M KCl solution. t_0 indicates the first frame when the bubble stays motionless beneath the HOPG surface. The wetting film between the air bubble and the HOPG surface then starts to drain and, after reaching a critical thickness, it ruptures. The three phase contact line, TPCL, is formed at $t_{rupture}$, and its perimeter increases, ensuring strong bubble attachment to the HOPG surface. Even though the wetting film ruptures in all three cases, the film drainage time, $t_{drainage}$, as well as the kinetics of the dewetting process, is different and dependent on the amount of air dissolved in the 10^{-1} M KCl solution. The time of film drainage, i.e. time from the moment when the air bubble does not move beneath HOPG surface (t_0) until the

wetting film ruptures ($t_{rupture}$), is the longest for degassed 10^{-1} M KCl solution ($t_{drainage}$ = 411.7 ± 154.2 ms, see black bars in Fig. 3A). The value of $t_{drainage}$ decreases by a factor of 2, down to 186.4 ± 98.6 ms, for an air bubble colliding with a HOPG surface in normal 10^{-1} M KCl solution. The most significant decrease in the time of film drainage is recorded for air saturated 10^{-1} M KCl solution. The value of $t_{drainage}$ is smaller by factor of 30 and it is only 6.1 ± 2.4 ms. The $t_{drainage}$ in air saturated 10^{-1} M KCl solution is in a good agreement with the film drainage times for air bubble colliding with HOPG surface in nitrogen saturated KCl solution (Wu et al., 2015).
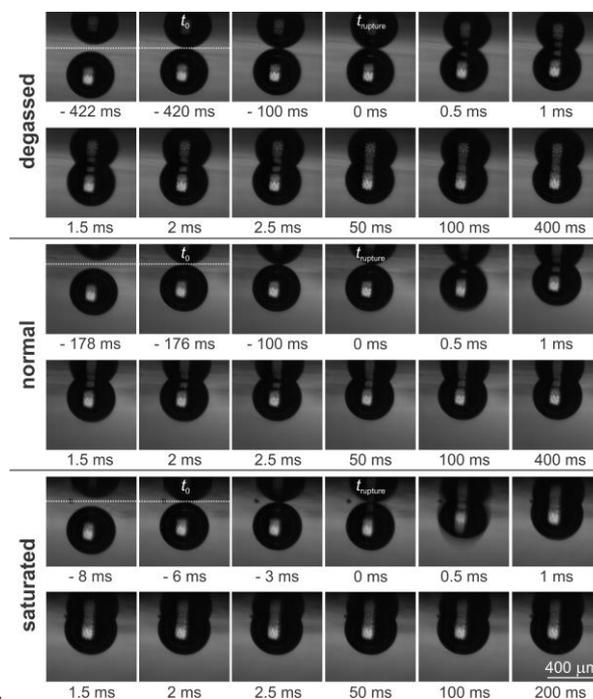
Fig. 2. A representative sequence of images showing the film rupture and dewetting at a freshly cleaved HOPG surface in: degassed 10^{-1} M KCl, pH 5.6 solution (top panel), normal 10^{-1} M KCl, pH 5.6 solution (middle panel), and air saturated 10^{-1} M KCl, pH 5.6 solution (bottom panel)

Once the TPCL is formed, and further dewetting occurs, the dewetting can be the best described by the evolution of the receding contact angle, θ_{rec}, as a function of time: the larger θ_{rec} and the faster this value is achieved the stronger is the bubble attachment to the solid surface. The top (degassed 10^{-1} M KCl solution) and middle (normal 10^{-1} M KCl solution) panels in Fig. 2 show a similar final (static) receding contact angle value, while the air bubble attached to HOPG surface in air saturated 10^{-1} M KCl solution shows a distinctively larger value of θ_{rec}.

A Matlab code was used to determine and extract receding contact angle values *vs* time. Detailed information about this process is given in the supporting information of (Kor et al., 2014). The dynamic receding contact angle values formed during the dewetting of HOPG surfaces in degassed (empty circles), normal (grey circles), and air saturated (black circles) 10^{-1} M KCl solution are given in Fig. 3B. One clear difference between the three cases occurs in first stage of the dewetting process: the dewetting is the slowest (with the least steep slope of the θ_{rec} *vs* t graph) for the degassed 10^{-1} M KCl solution. The static θ_{rec} is not reached until 20-25 ms after the wetting film rupture. The dewetting is faster in normal 10^{-1} M KCl solution and the static θ_{rec} is reached after 3-7 ms from the wetting film rupture. The fastest dewetting (with the steepest slope of the θ_{rec} *vs* t graph) occurs in air saturated 10^{-1} M KCl solution. The static θ_{rec} is reached almost instantaneously, within 1-2 ms from the wetting film rupture. The static receding contact angles are, within the experimental error, the same for air bubbles attached to HOPG surface in degassed (51 ± 4 °) and normal (52 ± 5 °) 10^{-1} M KCl solutions (compare grey bars in Fig. 3A and data for longer, i.e. 50 ms, times in Fig. 3B). The static receding contact angle is significantly higher (63 ± 6 °) for the air bubble attached to HOPG surface in air saturated 10^{-1} M KCl. The fact that: (*i*) the film drainage is significantly shorter, (*ii*) the dewetting kinetics is

significantly faster, and (*iii*) the static receding contact angle value is the highest in air saturated 10^{-1} M KCl solution indicate that dissolved air must play a significant role in all these processes.
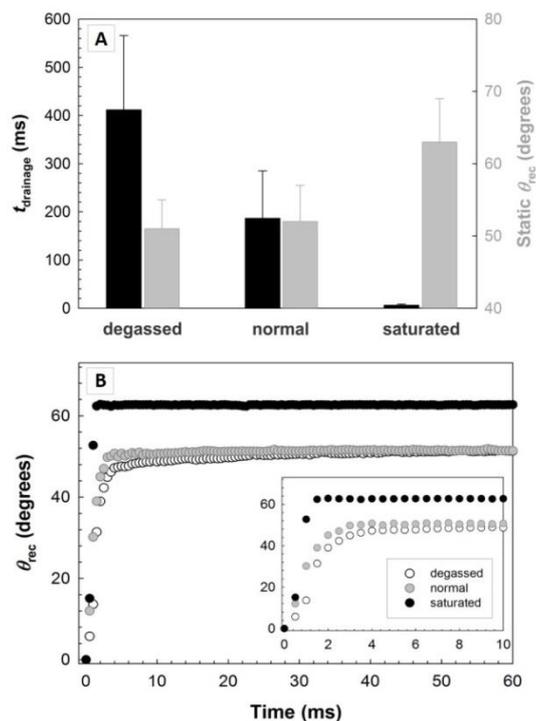
Fig. 3. Panel A – time of the wetting film drainage, $t_{drainage}$ (black bars, left y-axis) and static receding contact angle, θ_{rec} (grey bars, right y-axis) in degassed, normal, and air saturated 10^{-1} M KCl, pH 5.6 solution. Panel B – dynamic receding contact angle formed during the dewetting of HOPG surface in degassed (empty circles), normal (grey circles), and air saturated (black circles) 10^{-1} M KCl, pH 5.6 solution. Bubble radius, $R_b = 201 \pm 11$ μm
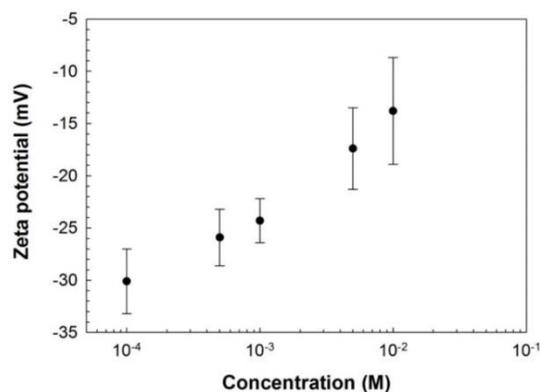
Fig. 4. Zeta potential determined from streaming potential measurements for HOPG surface in degassed KCl solution of different concentration at pH 5.6

The zeta potential for the HOPG surface at pH 5.6 is negative (see Fig. 4). Since the zeta potential cannot be measured at high ionic strengths we determined its value at lower salt concentrations and extrapolated the zeta potential value for 10^{-1} M KCl to be c.a. – 8 mV. The zeta potential of an air bubble in 10^{-1} M NaCl (assuming there is no specific Na$^+$ ion adsorption at solution-air interface there should be no difference between NaCl and KCl solutions) at pH 5.6 is c.a. – 12 mV (Yang et al., 2001). The negative zeta potentials at both air-solution and solution-HOPG interfaces will result in repulsive electric double layer forces between these surfaces (see dashed line in Fig. 5). This means the electrostatic component of the total force stabilises the wetting film at an HOPG surface, acting to prevent its rupture. On the other hand, it is worth noting that we have chosen high ionic strength, *I*,

equal to 10^{-1} to minimise the effect of electrostatic interactions. For $I = 10^{-1}$ the electric double layer forces are very short range (Debye length, $1/\kappa$, is 0.96 nm) and weak (zeta potential for solution-HOPG interface is - 8 mV, while the one for air bubble - 12 mV) – as clearly seen in Fig. 5. The Hamaker coefficient for carbon-water-air system is negative: $-5.68 \cdot 10^{-20}$ J (Donose et al., 2009). This results in repulsive van der Waals interactions (see black dotted line in Fig. 5 – van der Waals force is non-zero at film thicknesses as large as 20 – 30 nm). Since both electrical double layer and van der Waals forces are repulsive (as shown in Fig. 5), wetting film rupture between an air bubble and a HOPG surface is indeed paradoxical.
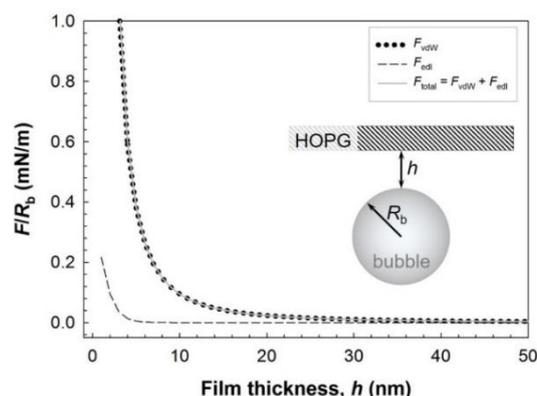
Fig. 5. The normalised (in respect to bubble radius, R_b) interaction forces between an air bubble and HOPG surface in 10^{-1} M KCl at pH 5.6 *vs* wetting film thickness, *h*. Non-retarded van der Waals interactions (dotted black line) were calculated for a sphere-flat surface geometry (Parsegian, 2005). The Hamaker coefficient used for carbon-water-air system was $-5.68 \cdot 10^{-20}$ J (Donose et al., 2009). The electrostatic interactions for the system were computed using constant potential boundary conditions and the Hogg-Healy-Fuerstenau (HHF) approximation (Hogg et al., 1966). The zeta potential value for bare surface HOPG (-8 mV) and -12 mV (Yang et al., 2001) were used in place of surface potentials, $R_b = 200$ μm

In our studies, the stability of the wetting films at HOPG surfaces decreases with the increase of air dissolved in 10^{-1} M KCl solution. The amount of dissolved air does not change the physicochemical parameters of bulk materials, hence should not affect Hamaker coefficient. However, it promotes nano-/submicro-metre bubble nucleation at hydrophobic surface such as HOPG. One of the first to propose that gas was able to exist in water in two forms: dissolved gas molecules and gas nuclei, of submicroscopic dimensions was Wrobel (Wrobel, 1952). He concluded that without the presence of gas nuclei, no bubble formation was possible, even at high solution saturation with gas. These findings explain why bubble formation is only possible where inhomogeneities, such as pre-existing gas nuclei or gas trapped in crevices of solid surface, are present in the thin liquid film. Even though HOPG is smooth it will have some local defects and inhomogeneities (i.e. terraces) where the nano-/submicro-metre bubble formation will occur. Where the HOPG surface is partially coated with small bubbles of height 10-80 nm (Zhang et al., 2006), i.e. greater than the Debye length at the HOPG-solution interface ($1/\kappa = 0.96$ nm) the initial air bubble-solution-HOPG interaction becomes an air bubble-solution-air nanobubble interaction, on those parts of the HOPG surface where nanobubbles reside. The probability of nano-/submicro-metre bubble nucleation at HOPG surfaces increases with the increase of the dissolved air in 10^{-1} M KCl solution, explaining the trend in the decreasing wetting film stability observed for solutions with increasing amount of dissolved air. This is consistent with early work of Wrobel (Wrobel, 1952), who concluded that the flotation rate and recovery of particles were found to be proportional to the amount of gas nuclei present in the system. With this in mind let us consider the balance of surface forces acting in the discussed systems. The forces acting in 10^{-1} M KCl between a macroscopic air bubble and air nanobubbles, i.e. across the foam film, are plotted in Fig. 6. Since the zeta (and surface) potential at both interfaces is the same (in sign and in magnitude) the electric double layer forces are repulsive (and due to high ionic strength weak and short range – see black dashed line in Fig. 6).
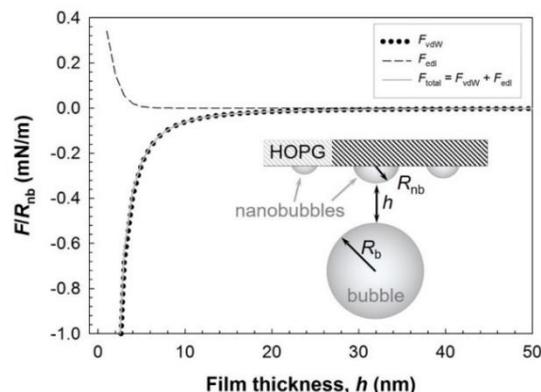
Fig. 6. The normalized (in respect to nanobubble radius, R_{nb}) interaction forces between an air bubble and nanobubble in 10^{-1} M KCl at pH 5.6 *vs* foam film thickness, h. Non-retarded van der Waals interactions (dotted black line) were calculated for the sphere-sphere geometry (Parsegian, 2005). The Hamaker coefficient used for air-water-air system was: 3.7×10^{-20} J (Israelachvili, 2011). The electrostatic interactions for the system were computed using constant potential boundary conditions and the Hogg-Healy-Fuerstenau (HHF) approximation (Hogg et al., 1966). The zeta potential of -12 mV (Yang et al., 2001) was used in place of surface potentials, $R_b = 200$ μm, $R_{nb} = 50$ nm

The Hamaker coefficient for air-water-air system is positive: 3.7×10^{-20} J (Israelachvili, 2011) and hence the van der Waals interactions are attractive. The van der Waals force is non-zero at film thicknesses as large as 20 nm (see black dotted line in Fig. 6). It is the dominating force in such systems, and hence the total force is also attractive (see grey solid line in Figure 6) and acts to destabilise the foam film and promote macroscopic air bubble attachment to a HOPG surface with resident nano-/submicro-metre bubbles. The presence of nano-/submicro-metre bubbles was reported to be responsible for the film rupture at other hydrophobic surfaces (Mahnke et al., 1999; Yang et al. 2003; Stöckelhuber et al., 2004; Slavchov et al., 2005; Mishchuk et al., 2006; Krasowska and Malysa, 2007a; Krasowska et al., 2007; Krasowska et al., 2009; Kosior et al., 2013), however none of the studied surfaces were as smooth as HOPG, therefore there was always an underlying effect of surface roughness. By choosing atomically smooth HOPG, performing experiments at high ionic strength, and gradually increasing the amount of air dissolved in 10^{-1} M KCl solution, we were able to decouple effects due to roughness and electrical double layer forces, with the observations being explainable solely by considering van der Waals interactions.

4. Conclusions

The stability of thin liquid films between HOPG and air bubbles in 10^{-1} M KCl solution under quasi-equilibrium conditions depends on the amount of air dissolved in the aqueous phase. The film becomes less stable (as indicated by shorter times needed for film drainage and rupture) with increasing amount of dissolved air. The kinetics of the dewetting process is also affected by the dissolved air: the dewetting is the fastest (and the final receding contact angle the largest) in the case of air saturated 10^{-1} M KCl. The instability of the thin liquid film is attributed to the attractive van der Waals interactions between a macroscopic air bubble and nano-/submicro-metre bubbles nucleated at the HOPG surface. The number (and size) of nucleated nano-/submicro-metre bubbles will likely increase with the amount of air dissolved in aqueous phase, resulting in faster thin liquid film rupture and macroscopic air bubble attachment to HOPG surface.

References

CHON U, C., OHL, C.-D., 2012. *Total-internal-reflection-fluorescence microscopy for the study of nanobubble dynamics*. Phys. Rev. Let., 109, 174501.

CONSIDINE, R.F., HAYES, R.A., HORN, R.G, 1999. *Forces measured between latex spheres in aqueous electrolyte: non-DLVO behavior and sensitivity to dissolved gas*. Langmuir, 15, 1657-59.

CRAIG, V.S.J., 2011. *Very small bubbles at surfaces - the nanobubble puzzle*. Soft Matter, 7, 40-48.

DONOSE, B. C., TARAN, E., HAMPTON, M.A., KARAKASHEV, S.I., NGUYEN. A.V., 2009. *Carbon nanotube air-bubble interactions studied by atomic force microscopy*. Adv. Powder Technol., 20, 257-261.

ERIKSSON, J.CH., LJUNGGREN, S., CLAESSON, P.M., 1989. *A phenomenological theory of long-range hydrophobic attraction forces based on a square-gradient variational approach*. J. Chem. Soc. Faraday Trans., 85, 163-176.

GERMAN, S. R, WU, X., AN, H., CRAIG, V.S.J., MEGA, T.L., ZHANG, X., 2014. *Interfacial nanobubbles are leaky: Permeability of the gas/water interface*. ACS nano, 8, 6193-6201.

GONG, W., STEARNES, J., FORNASIERO, D., HAYES, R.A., RALSTON, J., 1999. *The influence of dissolved gas on the interactions between surfaces of different hydrophobicity in aqueous media Part II. A spectroscopic study*. Phys. Chem. Chem. Phys., 1, 2799-2803.

HAMPTON, M.A., NGUYEN, A.V., 2010. *Nanobubbles and the nanobubble bridging capillary force*. Adv. Colloid Interface Sci., 154, 30-55.

HOGG, R., HEALY, T., FUERSTENAU, D.W., 1966. *Mutual coagulation of colloidal dispersions*. Trans. Faraday Soc., 62, 1638-1651.

ISHIDA, N., INOUE, T., MIYAHARA, M., HIGASHITANI, K., 2000. *Nano bubbles on a hydrophobic surface in water observed by tapping-mode atomic force microscopy*. Langmuir, 16, 6377-80.

ISRAELACHVILI, J N. 2011. *Intermolecular and Surface Forces*. Elsevier Science Publishing Co Inc, San Diego.

ISRAELACHVILI, J. N., PASHLEY, R.M., 1984. *Measurement of the hydrophobic interaction between two hydrophobic surfaces in aqueous electrolyte solutions*. J. Colloid Interface Sci., 98, 500-514.

ISRAELACHVILI, J., PASHLEY, R., 1982. *The hydrophobic interaction is long range, decaying exponentially with distance*. Nature, 300, 341-342.

JIANG, L., KRASOWSKA, M., FORNASIERO, D., KOH, P., RALSTON, J., 2010. *Electrostatic attraction between a hydrophilic solid and a bubble*. Phys. Chem. Chem. Phys., 12, 14527-14533.

KARPITSCHKA, S., DIETRICH, E., SEDDON, J.S.T., ZANDVLIET, H.J.W., LOHSE, D., RIEGLER, H., 2012. *Nonintrusive optical visualization of surface nanobubbles.* Phys. Rev. Let., 109, 066102.

KLASEBOER, E., MANICA, R., CHAN, D.Y.C., KHOO, B C., 2011. *BEM simulations of potential flow with viscous effects as applied to a rising bubble. Eng. Anal. Bound. Elem.*, 35, 489-494.

KOR, M., KORCZYK, P. M., ADDAI-MENSAH, J., KRASOWSKA, M., BEATTIE, D.A., 2014. *Carboxymethylcellulose Adsorption on Molybdenite: The Effect of Electrolyte Composition on Adsorption, Bubble-Surface Collisions, and Flotation'.* Langmuir, 30, 11975-11984.

KOSIOR, D., ZAWALA, J., KRASOWSKA, M., MALYSA, K., 2013. *Influence of n-octanol and a-terpineol on thin film stability and bubble attachment to hydrophobic surface.* Phys. Chem. Chem. Phys., 15, 2586-2595.

KRASOWSKA, M., KOLASINSKA, M., WARSZYNSKI, P., MALYSA, K., 2007. *Influence of polyelectrolyte layers deposited on mica surface on wetting film stability and bubble attachment.* J. Phys. Chem. C, 111, 5743-49.

KRASOWSKA, M., KRASTEV, R., ROGALSKI, M., MALYSA, K., 2007. *Air-facilitated three-phase contact formation at hydrophobic solid surfaces under dynamic conditions.* Langmuir, 23, 549-557.

KRASOWSKA, M., MALYSA, K., 2007a. *Kinetics of bubble collision and attachment to hydrophobic solids: I. Effect of surface roughness.* Int. J. Miner. Proces., 81, 205-216.

KRASOWSKA, M., MALYSA, K., 2007b. *Wetting films in attachment of the colliding bubble.* Adv. Colloid Interface Sci., 134, 138-150.

KRASOWSKA, M., ZAWALA, J., MALYSA, K., 2009. *Air at hydrophobic surfaces and kinetics of three phase contact formation.* Adv. Colloid Interface Sci., 147, 155-169.

LOU, S.-T., OUYANG, Z.-Q., ZHANG, Y., LI, X.-J., HU, J., LI, M.-Q., YANG, F.-J., 2000. *Nanobubbles on solid surface imaged by atomic force microscopy.* J. Vac. Sci. Technol. B, 18, 2573-2575.

LOU, S., GAO, J., XIAO, X., LI, X., LI, G., ZHANG, Y., LI, M., SUN, J., LI, X., HU, J., 2002. *Studies of nanobubbles produced at liquid/solid interfaces.* Mater. Charact., 48, 211-214.

MAHNKE, J., SCHULZE, H.J., STÖCKELHUBER, K.W., RADOEV, B., 1999. *Rupture of thin wetting films on hydrophobic surfaces: Part I: methylated glass surfaces.* Colloids Surf. A, 157, 1-9.

MALYSA, K., KRASOWSKA, M., KRZAN, M., 2005. *Influence of surface active substances on bubble motion and collision with various interfaces.* Adv. Colloid Interface Sci., 114, 205-225.

MALYSA, K., ZAWALA, J., KRZAN, M., KRASOWSKA, M., 2011. *Bubbles Rising in Solutions, Local and Terminal Velocities, Shape Variations and Collisions with Free Surface.* Brill.

MEZGER, M., REICHERT, H., SCHÖDER, S., OKASINSKI, J., SCHRÖDER, H., DOSCH, H., PALMS, D., RALSTON, J., HONKIMÄKI, V., 2006. *High-resolution in situ x-ray study of the hydrophobic gap at the water–octadecyl-trichlorosilane interface.* Proc. Nat. Acad. of Sci., 103, 18401-1804.

MISHCHUK, N., RALSTON, J., FORNASIERO, D., 2006. *Influence of very small bubbles on particle/bubble heterocoagulation.* J. Colloid Interface Sci., 301, 168-175.

NGUYEN, A.V., RALSTON, J., SCHULZE, H.J., 1998. *On modelling of bubble–particle attachment probability in flotation.* Int. J. Miner. Proces., 53, 225-249.

NGUYEN, A.V., SCHULZE, H.J., 2003. *Colloidal science of flotation.* CRC Press.

PARKER, J.L., CLAESSON, P.M., ATTARD, P., 1994. *Bubbles, cavities, and the long-ranged attraction between hydrophobic surfaces.* J. Phys. Chem., 98, 8468-8480.

PARSEGIAN, V.A., 2005. *Van der Waals forces: a handbook for biologists, chemists, engineers, and physicists.* Cambridge University Press.

ROGERS, M.H., LANCE, G.N., 1960. *The rotationally symmetric flow of a viscous fluid in the presence of an infinite rotating disk.* J. Fluid Mech., 7, 617-631.

SIDES, P.J., NEWMAN, J., HOGGARD, J.D., PRIEVE, D.C., 2006. *Calculation of the streaming potential near a rotating disk.* Langmuir, 22, 9765-9769.

SIDES, P.J., PRIEVE, D.C., 2013. *Surface conductivity and the streaming potential near a rotating disk-shaped sample.* Langmuir, 29, 13427-13432.

SIMONSEN, A.C., HANSEN, P.L., KLÖSGEN, B., 2004. *Nanobubbles give evidence of incomplete wetting at a hydrophobic interface.* J. Colloid Interface Sci, 273, 291-299.

SLAVCHOV, R., RADOEV, B., STÖCKELHUBER, K.W., 2005. *Equilibrium profile and rupture of wetting film on heterogeneous substrates.* Colloids Surf. A., 261, 135-140.

SNOSWELL, D.R.E., DUAN, J., FORNASIERO, D., RALSTON, J., 2003. *Colloid stability and the influence of dissolved gas.* J. Phys. Chem. B, 107, 2986-2994.

STEITZ, R., GUTBERLET, T., HAUSS, T., KLÖSGEN, B., KRASTEV, R., SCHEMMEL, S., SIMONSEN, A.C., FINDENEGG, G.H., 2003. *Nanobubbles and their precursor layer at the interface of water against a hydrophobic substrate.* Langmuir, 19, 2409-2418.

STÖCKELHUBER, K.W., RADOEV, B., WENGER, A., SCHULZE, H.J., 2004. *Rupture of wetting films caused by nanobubbles.* Langmuir, 20, 164-168.

TREFALT, G., SZILAGYI, I., ONCSIK, T., SADEGHPOUR, A., BORKOVEC, M., 2013. *Probing colloidal particle aggregation by light scattering.* Int. J. Chem., 67, 772-776.

WROBEL, S. 1952. *The adsorption of nuclear gas - its role in froth flotation'.* Mine Quarry Eng., 313-317.

WU, J., DELCHEVA, I., NGOTHAI, Y., KRASOWSKA, M., BEATTIE, D.A., 2015. *Bubble-surface interactions with graphite in the presence of adsorbed carbomethylcellulose.* Soft Matter, 11, 587-599.

YANG, C., DABROS, T., LI, D., CZARNECKI, J., MASLIYAH, J.H., 2001. *Measurement of the Zeta Potential of Gas Bubbles in Aqueous Solutions by Microelectrophoresis Method.* J. Colloid Interface Sci., 243, 128-135.

YANG, J., DUAN, J., FORNASIERO, D., RALSTON, J., 2003. *Very Small Bubble Formation at the Solid−Water Interface.* J. Phys. Chem. B, 107, 6139-6147.

YANG, J., DUAN, J., FORNASIERO, D., RALSTON, J., 2007. *Kinetics of CO_2 nanobubble formation at the solid/water interface.* Phys. Chem. Chem. Phys., 9, 6327-6332.

YOON, R.-H., MAO, L., 1996. *Application of extended DLVO theory, IV: derivation of flotation rate equation from first principles.* J. Colloid Interface Sci., 181, 613-626.

ZAWALA, J., KOSIOR, D., MALYSA, K., 2015. *Formation and influence of the dynamic adsorption layer on kinetics of the rising bubble collisions with solution/gas and solution/solid interfaces.* Adv. Colloid Interface Sci., 222, 765-778.

ZAWALA, J., SWIECH, K., MALYSA, K.. 2007. *A simple physicochemical method for detection of organic contaminations in water.* Colloids Surf. A., 302, 293-300.

ZHANG, L., ZHAO, B., XUE, L., GUO, Z., DONG, Y., FANG, H., TAI, R., HU, J., 2013. *Imaging interfacial micro-and nano-bubbles by scanning transmission soft X-ray microscopy.* J. Synchr. Rad., 20, 413-418.

ZHANG, X.H., MAEDA, N., CRAIG, V.S.J., 2006. *Physical properties of nanobubbles on hydrophobic surfaces in water and aqueous solutions.* Langmuir, 22, 5025-5035.